In-Situ Deposition of Alkali and Alkaline Earth Hydride Thin Films To Investigate the Formation of Reactive Hydride Composites

10 AUTHORS, INCLUDING:

Marta Gonzalez-Silveira
Autonomous University of Barcelona

28 PUBLICATIONS **383** CITATIONS

SEE PROFILE

Robin Gremaud
ABB

42 PUBLICATIONS **922** CITATIONS

SEE PROFILE

Loic Dupont
Université de Picardie Jules Verne

128 PUBLICATIONS **7,137** CITATIONS

SEE PROFILE

Bernard Dam
Delft University of Technology

259 PUBLICATIONS **4,563** CITATIONS

SEE PROFILE

In-Situ Deposition of Alkali and Alkaline Earth Hydride Thin Films To Investigate the Formation of Reactive Hydride Composites

**M. Gonzalez-Silveira,*,†,‡ R. Gremaud,¶ H. Schreuders,§ M. J. van Setten,*,‖ E. Batyrev,†
A. Rougier,⊥ L. Dupont,⊥ E. G. Bardají,‖ W. Lohstroh,‖ and B. Dam§**

Faculty of Sciences, Department of Physics and Astronomy, Condensed Matter Physics, Vrije Universiteit, De Boelelaan 1081, 1081 HV Amsterdam, The Netherlands, Grup de Nanomaterials i Microsistemes, Department of Physics, Universitat Autonoma de Barcelona, 08193 Bellaterra, Spain, EMPA, Swiss Federal Laboratories for Materials Testing and Research, Laboratory 138, Hydrogen and Energy, Überlandstrasse 129, CH-8600 Dübendorf, Switzerland, MECS, Department of Chemical Engineering, Delft University of Technology, Julianalaan 136, 2600 GA Delft, The Netherlands, Institute of Nanotechnology, Karlsruhe Institute of Technology, D-76021 Karlsruhe, Germany, and Laboratoire de Réactivité et de Chimie des Solides, CNRS UMR-6007, Université de Picardie Jules Verne, 33 Rue Saint Leu, 80039 Cedex, France

We investigate the critical steps in the formation of $Ca(BH_4)_2$ starting from CaH_2-MgB_2 thin films. As a first step, thin films of CaH_2 are successfully deposited by reactive sputtering using a mixture of Ar/H_2 as sputter plasma. The films are analyzed by transmission electron microscopy (TEM) and by optical spectrophotometry. The calculated dielectric functions for CaH_2, Ca, and $Ca(OH)_2$ are used to reproduce the optical measurements and to check the quality of the films. The calculation of the dielectric functions of the hydrides is performed by first solving the quasi-particle equation in the GW_0 approximation to the Hedin equations and by second solving the equation of motion for an electron hole pair, the Bethe Salpeter equation. In this way, the exciton effects are also included in the dielectric function. The same procedure is used on NaH films to show the validity of the method. The experimental optical gaps obtained for the two hydrides (5.8 ± 0.1 eV for NaH and 5.2 ± 0.1 eV for CaH_2) fit considerably well with the theoretical calculations. MgB_2 films have been deposited at room temperature by sputtering using a MgB_2 target. X-ray photoelectron spectroscopy (XPS) shows that boron is bound to the MgB_2 phase while there is a small amount of free magnesium in excess which can be partly oxidized. Co-sputtered and multilayered CaH_2-MgB_2 thin films are investigated using high-pressure differential scanning calorimetry (HP-DSC). Both starting configurations show an exothermic reaction around 628 K during hydrogenation at 100 and 140 bar H_2, which is consistent with the formation of $Ca(BH_4)_2$, with a more complete reaction in the co-sputtered case. However, the nanocrystalline/amorphous nature of the product does not allow further structural characterization. Despite optimal atomic mixing provided by the thin film approach, the reaction still occurs at high temperature and pressure confirming the preeminence of nucleation over diffusion processes for the formation of calcium borohydride in this complex reactive synthesis.

Introduction

High-volume and gravimetric capacities as well as adequate kinetic and thermodynamic properties are the main targets in the search for a suitable solid state hydrogen storage material. Complex hydrides present interesting qualities regarding their storage capacity, but from a thermodynamic point of view, they are still far from the desirable operation conditions. A promising route to lower the reaction enthalpy in these kind of compounds is the combination of the complex hydrides with other light-metal hydrides.[1] These systems are denoted reactive hydride composites (RHC) when all the compounds react during the absorption/desorption process.[2] Interesting examples of RHC with high storage capacities[3] are composites with borohydrides

combined with light hydrides, such as $MgH_2 + NaBH_4$,[4] $MgH_2 + LiBH_4$,[5–7] $MgH_2 + Ca(BH_4)_2$, which is reversible,[8,9] and $CaH_2 + LiBH_4$.[10] The presence of the light hydride destabilizes the complex hydride by reducing the dehydrogenation/hydrogenation enthalpy due to the formation of compounds such as MgB_2[11,12] or CaB_6[13,14] on desorption. Even the combination of complex hydrides can produce a similar effect.[15,16] However, kinetic limitations appear to dominate the reaction since high pressures and temperatures are still necessary for these materials to react. Hence, we here report on our efforts to reproduce the RHC reactions in a thin film. Apart from nanorange microstructure, which diminishes considerably interdiffusion distances, the versatility of thin films is also a remarkable advantage. The reaction can be localized; for instance, in a multilayer structure the reaction is expected to take place first in the interfaces. The localization of the reaction gives the possibility of placing catalysts in a well-defined surrounding, which facilitates the analysis of the mechanism by which they operate. A co-sputtered film, on the other hand, allows us to analyze the reaction under conditions of optimal mixing.

* To whom correspondence should be addressed. E-mail: marta.gonzalez@uab.cat; michiel.setten@kit.edu.
† Vrije Universiteit Amsterdam.
‡ Universitat Autonoma de Barcelona.
¶ EMPA.
§ Delft University of Technology.
‖ Karlsruhe Institute of Technology.
⊥ Université Amsterdam.

However, the production of the relevant reactant layers is by no means trivial. Reactive deposition techniques have proven to be a good option for the deposition of hydride thin films. The growth of MgH_2,[17] Mg_2NiH_4,[18] LiH,[19] and, more recently, the complex metal hydride $NaAlH_4$[20] has been possible by using a source of atomic hydrogen. TiH_2,[21] LiH,[22] and very thin films of MgH_2[23] have also been deposited by introducing molecular hydrogen gas in the chamber during the evaporation[21,23] or in the sputter plasma.[22] Hydride thin films can easily be analyzed by optical spectrophotometry, which has proven to be a very useful technique for the characterization of this kind of films when combined with the theoretical calculation of the corresponding optical properties.[17,18,20,24,25] The growth of MgB_2 films is also not trivial. Because of the interest that was generated by the discovery of the superconducting properties of MgB_2, there have been many different approaches for the deposition of these films (e.g., refs 26–28).

In this study, we focus our attention mainly on the deposition and characterization of the reactant layers CaH_2 and MgB_2. The hydride films are successfully deposited by means of reactive sputtering using molecular hydrogen as the reactive gas. We use the combination of optical spectrophotometry measurements and the simulation of the optical properties to evaluate the quality of the hydride. To show the effectiveness of the method, we use the same approach on reactively sputtered NaH thin films. After the deposition of proper reactant phases, we use two different configurations: CaH_2–MgB_2 co-sputtered films and multilayers to study the formation of $Ca(BH_4)_2$ via the reaction $CaH_2 + MgB_2 + 4H_2 \rightarrow Ca(BH_4)_2 + MgH_2$. High-pressure differential scanning calorimetry (HP-DSC) allows us to perform the hydrogenation treatment under controlled high hydrogen pressure and temperature conditions. The comparison of our thin film data with the results published for bulk samples indicates that diffusion is not a limiting factor in the RHC reaction mechanism.

Experimental Section

CaH_2 and NaH thin films are deposited at room temperature by means of reactive radio frequency (RF) sputtering from pure Ca and Na targets at a base pressure of 10^{-7} Pa. The plasma is generated from a mixture of argon and hydrogen with a flow of Ar:2.5 and H_2:5.0 × 10^{-7} m^3/s at standard temperature and pressure (293.15 K and 101.325 kPa). Using a power of 50 W, a target-sample distance of approximately 0.15 m, and 0.5 Pa of pressure, the deposition rates are 0.23 and 0.1 Å/s for CaH_2 and NaH, respectively. MgB_2 films are obtained by means of direct current (DC) sputtering from a MgB_2 target supplied by Edison Spa, Milano, Italy, which was manufactured according to the reactive liquid Mg infiltration (Mg-RLI) process.[29] The films are grown at room temperature using a power of 120 W with no further annealing after the deposition. Two different sets of MgB_2 films are deposited using Ar or Ar/H_2 plasmas. Co-sputtered CaH_2–MgB_2 films are deposited using always Ar/H_2 plasma to achieve the formation of the hydride in the mixture. The optical analysis is performed by means of a PerkinElmer Lambda 900 UV/visible/near infrared (NIR) spectrophotometer (0.495–6.51 eV) on hydride films with nominal thicknesses of 200 nm deposited on quartz substrates. After deposition, the samples are transferred to a glovebox connected to the deposition system. The quartz substrate with the film is mounted as one of the windows of a sealed cell. This cell is transferred outside the glovebox and can be placed directly in the spectrophotometer. The cell can be evacuated and filled with hydrogen. Optical reflectance R and transmittance T spectra are recorded at near-

TABLE 1: Lattice Parameters Obtained from the Optimization of the Structures

	a	b	c
Ca	5.58 Å	5.58 Å	5.58 Å
CaH_2	5.9247 Å	3.5833 Å	6.8022 Å
$Ca(OH)_2$	3.6146 Å	3.6146 Å	4.9372 Å

normal incidence. For transmission electron microscopy (TEM) analysis, the films are deposited on 30 nm silicon nitride window membranes. Selected area electron diffraction (SAED) patterns are recorded with a Tecnai F20 at a camera length of 0.2 m and an acceleration voltage of 200 KeV. The so-obtained powder SAED patterns are treated with Process Diffraction software[30] to draw the corresponding X-ray diffraction-like diagrams that can be indexed using the Joint Committee on Powder Diffraction Standards database files. The analysis of the reactant layers has been completed with Rutherford backscattering spectrometry (RBS) and X-ray photoelectron spectroscopy (XPS). The XPS spectra were obtained using Al Kα radiation (1486.6 eV) in a Multiprobe XP ultra high vacuum Omicron system on samples deposited on Si substrates with a nominal thickness of 100 nm. In this case, no Pd was deposited on top of the samples, and surface C was used for the calibration of the system. Depth profiles are obtained by sputtering the films with Ar^+ ions (1 keV, 10 mA). RBS measurements were performed using 2 MeV He atoms on films deposited on glassy C substrates to get the signal from the substrate at very low energies. On top of the hydride film, a 15 nm layer of Pd protects the sample from oxidation during the handling. The RBS data have been simulated using the software XRUMP.[31]

High-pressure differential scanning calorimetry measurements on pure CaH_2 and MgB_2 films, as well as co-sputtered films and multilayers, are performed in a high-pressure differential scanning calorimeter (HP-DSC) 204 Netzsch. The multilayer consists of eight repetitions of the sequence [30 nm CaH_2 + 0.2 nm Ti + 15 nm MgB_2 + 0.2 nm Ti]. The sample is covered with an extra layer of 5 nm of MgB_2. The MgB_2 layers are deposited using pure Ar plasma in this case. For the cosputtered film, we use Ar/H_2 plasma to deposit a 500 nm film of CaH_2 + MgB_2 with 1% of Ti as a dopant. The ratio between CaH_2 and MgB_2 is measured to be close to one. The addition of Ti in both cases was considered because of its demonstrated catalytic effect in the formation of $NaAlH_4$[32] although Ti is often introduced in a different form, for example, Ti isopropoxide[8] or $TiCl_3$[14] in $Ca(BH_4)_2$. To avoid the oxidation of the MgB_2 top layer, the samples are kept in an inert atmosphere until the moment of the measurement. The films are deposited on 20 μm thin Cu foils to minimize the influence of the substrate in the measurement. Small pieces of the foil are introduced in Al crucibles fitted with Al_2O_3 liners. The samples are handled at all times in an argon-filled glovebox with partial pressures of oxygen and water below 1 ppm. The hydrogenation treatment consists of a temperature ramp from room temperature up to 773 K with a heating rate of 5 K/min under a static pressure of 10^7 and 1.5 × 10^7 Pa H_2.

Computational Methods

First principles calculations are carried out with the Vienna ab initio simulation package (VASP)[33–35] using the projector augmented wave method.[36,37] The structure of NaH was used as published previously.[24] In the case of Ca, CaH_2,[38] and $Ca(OH)_2$, the structures were fully optimized using the PW91 generalized gradient approximation for the exchange correlation.[39] The resulting lattice parameters (see Table 1) and atomic

Formation of Reactive Hydride Composites

J. Phys. Chem. C, Vol. 114, No. 32, 2010 **13897**

TABLE 2: Space Group and Wickoff Positions for the Crystal Structures of Ca, CaH$_2$, and Ca(OH)$_2$

	space group	atom	Wickoff position	coordinates	
Ca	$Im\bar{3}m$	Ca	1a		
CaH$_2$	$Pnma$	Ca	4c	$x = 0.2396$	$z = 0.1102$
		H1	4c	$x = 0.3556$	$z = 0.4273$
		H2	4c	$x = 0.9745$	$z = 0.6768$
Ca(OH)$_2$	$P\bar{3}m1$	Ca	1a		
		O	2d		$z = 0.7673$
		H	2d		$z = 0.5703$

TABLE 3: Computational Details: k-Point Meshes (Gamma Centered), Kinetic Energy Cutoff for the Wave Function Expansion, Number of Bands in the DFT Calculation, Kinetic Energy Cutoff for the Response Functions, and Number of Bands on Which the Excitons Are Calculated

	k-points	DFT cutoff	DFT bands	GW cutoff	exciton bands
Ca	G 64 × 64 × 64	128.5	30	n.a.	n.a.
NaH	G 16 × 16 × 16	400	100	100	4
CaH$_2$	G 4 × 6 × 4	312.5	160	100	10
Ca(OH)$_2$	G 6 × 6 × 6	400	168	100	10

positions (see Table 2) are all within 2% of the experimental values.

After structure optimization, the dielectric functions of the semiconductors are calculated in three steps. In the first step, density functional theory (DFT) calculations, in the local density approximation (LDA) for the exchange correlation, are used to calculate the initial wave functions and the screening as input for the GW calculations. In the second step, we perform the GW calculation. Here, we only update the energy levels that enter the Greens function to self-consistency as the wave functions and the screening are kept at DFT-random phase approximation (RPA) level. The corresponding properties are denoted by GW$_0$. Two hundred empty bands are sufficient for convergency for the GW$_0$ calculations and the DFT calculations to generate the initial wave functions for the GW$_0$ calculations. In the final step, the GW$_0$ results are used to calculate the two-particle exciton spectrum. To this end, vertex corrections are included by using a second iteration of the Hedin equations[40–42] using the Bethe-Salpeter approach in the Tamm-Dancoff approximation. The calculation of the exciton spectrum is performed taking eight empty energy bands into account. The above-described method is used as incorporated in the VASP code.[43–46] For Ca metal, the dielectric function is dominated by intraband transitions. These contributions are obtained for the calculated plasma frequency and are combined with interband dielectric function at DFT-RPA level as described in refs 47 and 48. For all systems, k-point meshes with a spread of 0.03 Å in each direction were needed to reach converged dielectric functions. For a summary of the computational details, see Table 3.

Results and Discussion

Reactant Films: CaH$_2$, NaH, and MgB$_2$ Films. As a first characterization, the as-deposited hydride thin films of CaH$_2$ and NaH were analyzed by optical spectrophotometry. Figure 1 shows the recorded optical transmittance and reflectance of the films. Both hydrides are insulators with a band gap beyond the visible spectrum. The experimental optical gap has been extracted from the intersection of T equal to zero and the slope of the transmission curve at the beginning of the gap. We find 5.8 ± 0.1 eV for NaH and 5.2 ± 0.1 eV for CaH$_2$; the latter is
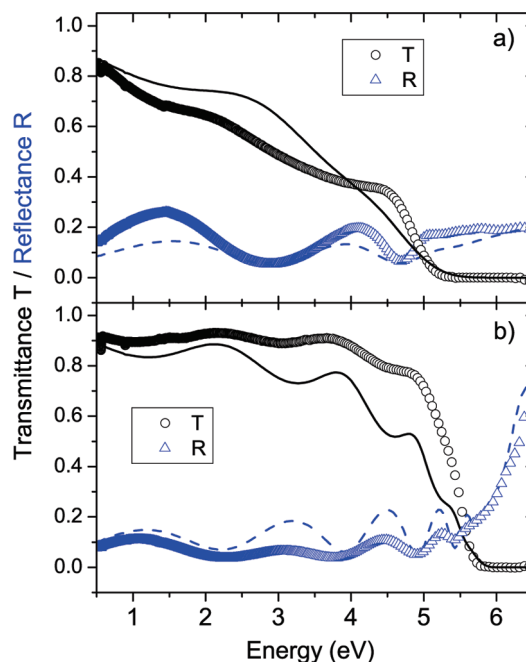
Figure 1. Experimental (symbols) and simulated (lines) data from the transmittance and reflectance of (a) CaH$_2$ and (b) NaH films.

in complete accordance with the ~5 eV gap found by Weaver et. al.[49] The transmittance and reflectance curves for NaH and CaH$_2$ have also been simulated using the software SCOUT,[50] which uses the dielectric functions of the materials to calculate the optical response (lines in Figure 1). For this, the dielectric functions were calculated using GW$_0$ + BSE method as described in the Computational Methods section. The best fit between experimental and simulated data has been obtained considering thicknesses of 120 nm for CaH$_2$ and 150 for NaH. NaH films were used as a probe to test the reliability of the calculation method. The significant agreement between experiment and simulation in the case of NaH demonstrates that the combination of optical spectrophotometry with the simulation of the optical data using first principles for the calculation of the electronic properties of the material is a reliable method for the evaluation of the quality of the hydride films. In the case of CaH$_2$, the agreement between experimental data and the simulation using the calculated dielectric functions is also considerable especially the size of the band gap. The simulated transmittance of an equivalent film with inclusions of metallic Ca in the CaH$_2$ matrix has also been calculated using the Bruggeman model.[51] When considering 5% of metallic Ca in the film, there is already a clear difference in the optical response at low energies (see Figure 2). Also for smaller fractions of metallic Ca, 1−2%, the correspondence between the experimental and simulated curves does not compare significantly better to the experimental curve than the one simulated for pure CaH$_2$. Although it is still possible that the films contain a small amount of unreacted Ca, we conclude, according to these optical data, that this will not be more than 5%. In contrast to MgH$_2$ films,[17] an almost complete hydrogenation of the Ca can therefore be achieved without the need of an atomic hydrogen source.

The samples were then exposed to 1 bar H$_2$ at room temperature for 3 h. This did not lead to any significant change in the optical curves from which we conclude that no further hydrogenation of the films takes place under these conditions. The CaH$_2$ film samples were also exposed to air after the measurement. As can be seen in Figure 2, the transmittance
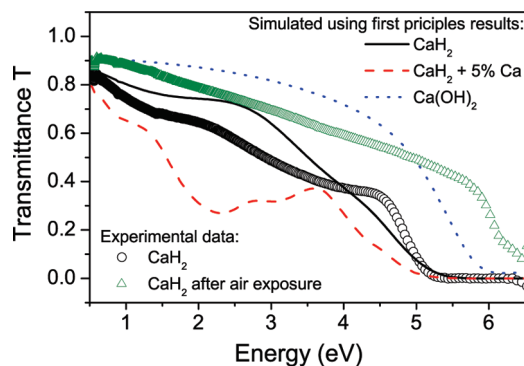
Figure 2. Experimental data for CaH_2 (circles) and CaH_2 after air exposure (triangles). The different lines correspond to the simulations of pure CaH_2 (solid), CaH_2 + 5% Ca (dashed), and $Ca(OH)_2$ (dotted) using first principles.
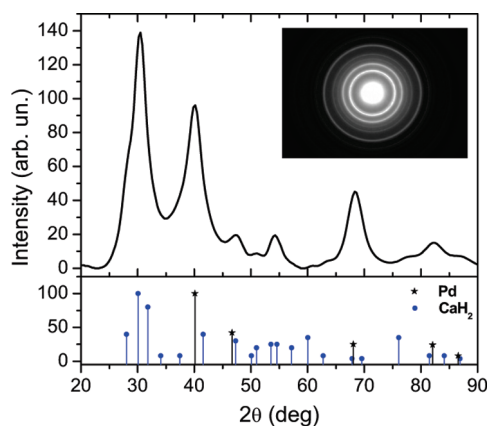

Figure 3. (top) SAED pattern for a 30 nm CaH_2 film covered with 4 nm of Pd. (bottom) Process diffraction treatment of the SAED pattern with indications of the CaH_2 and Pd powder diffraction files from the Joint Committee of Powder Diffraction Society (JCPDS) calculated using λ = 1.54 Å.
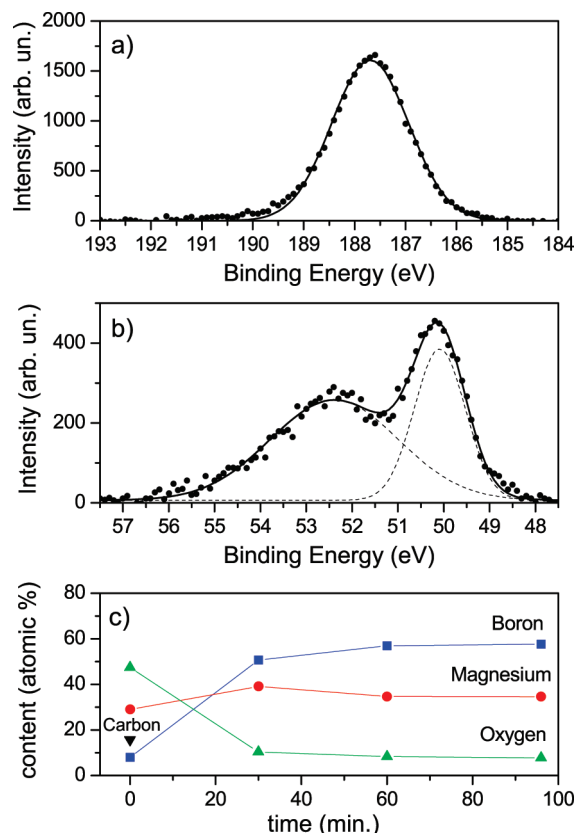

Figure 4. B 1s (a) and Mg 2p (b) spectra measured after 100 min of Ar etching on a 100 nm thin film of MgB_2 deposited with Ar plasma. The points show the experimental data. The curves are fitted to Gaussian line shape (dashed and continuous lines). (c) Composition profile as function of etching time for Mg, B, O, and C.

shows a shift to higher energies of the band gap of approximately 2 eV. This is probably due to the formation of calcium oxide, which has an optical gap of 6.9 eV.[52] $Ca(OH)_2$, on the contrary, has a gap around 5.8 eV as can be seen in the simulation of the optical transmittance of this phase (Figure 2). This value is too low for considering the formation of the hydroxide as a majority product of the reaction. When covering the samples with 10 nm of Pd, no change takes place in the hydride films immediately after air exposition.

The pure CaH_2 films have also been observed by TEM using plan view mode. This mode only allows the vision of the top Pd film showing crystalline grains with sizes around 10 nm. The SAED analysis of the sample, however, allows the observation of the diffraction rings from a polycrystalline CaH_2 film (see Figure 3) with no presence of other phases apart from polycrystalline Pd from the top layer as was expected from the optical measurements. No determination of the grain size was possible with this technique.

To analyze the quality of the MgB_2 films, we mainly rely on XPS. This technique resolves the chemical state of Mg and B and reveals the formation of oxides in the film. The samples, with no protective layer, were sputtered with Ar^+ ions for 100 min until a constant profile was obtained for all the components. All the spectra are fitted with Gaussian functions after subtracting a baseline. The B 1s spectra, shown in Figure 4a, presents one single peak at 187.7 eV. The binding energy is in the range of 187.7−188.2 eV attributed to B in MgB_2.[53,54] In the case of

Mg 2p, the spectra show two peaks, one at 50.1 eV and another at 52.4 eV (Figure 4b). The peak at lower energy can be assigned to metallic Mg (49.3[53]−49.8 eV[54]) or to MgO (48.9[55]−50.5 eV[54]), and the one at higher binding energy is closer to MgB_2 (51.3[53]−51.7 eV[54]). The distribution of the area for these two peaks shows that 37% of the Mg present in the film is not bound forming the MgB_2 phase. Considering the total percentages shown in Figure 4c (57% of B, 35% of Mg) after the sputtering of the film, we obtain a ratio of 2:1.23 of B:Mg. As will be shown later, this result is consistent with the Mg in excess observed by RBS in the films deposited using pure Ar plasma. Nevertheless, the ratio becomes 2:0.78 instead of 2:1 for B:Mg when considering only the percentage of bound Mg. Thus, 23% of the B is not bound to MgB_2. This B in excess probably corresponds to pure B, which has a binding energy around 186.9 eV.[54] The contribution of free B to the B 1s spectra is not visible probably because of the proximity between the energies corresponding to bound and unbound B. When analyzing the O 1s spectra (not shown), we obtain a small peak at 531 eV which matches with both boron (531.5 eV for B_2O_3[55]) and magnesium oxide (531 eV for MgO[54]). Since no oxide peaks can be distinguished in the B 1s spectra (192.9 eV[55]), the oxygen is probably oxidizing part of the free Mg in the film. Figure 4c shows that after sputtering the sample for almost 100 min with Ar^+ ions, the oxygen present in the film decreases from a 47% to less than 10%. Without any protective layer, most of this oxygen was probably absorbed after the deposition of the film.[56] The systematic shift toward lower energies of all the peaks can be due to the calibration of the system, which was performed using the C present on the surface of the films.
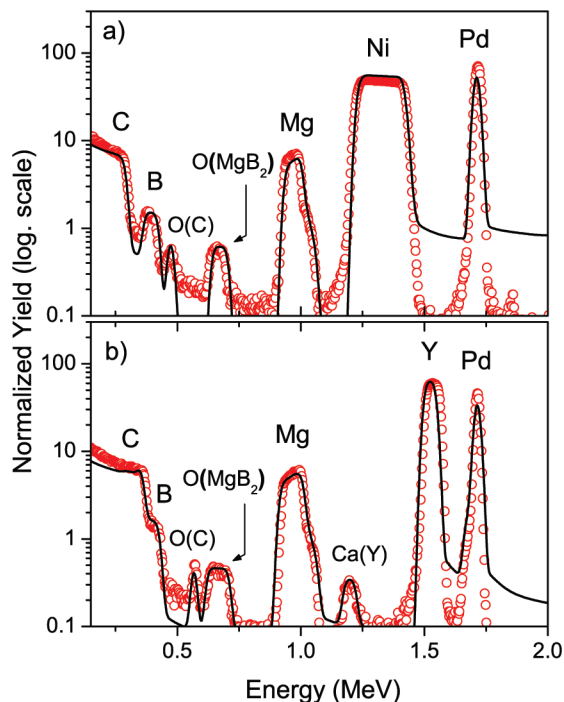
Formation of Reactive Hydride Composites

J. Phys. Chem. C, Vol. 114, No. 32, 2010 **13899**

Figure 5. RBS experimental data (circles) and simulation (line) from (a) 200 nm of MgB_2 deposited with an Ar plasma covered with a buffer layer of 150 nm Ni; (b) 200 nm of MgB_2 deposited with an Ar/H_2 plasma covered with a buffer layer of 100 nm Y. The brackets indicate the layers where the corresponding impurities can be found.
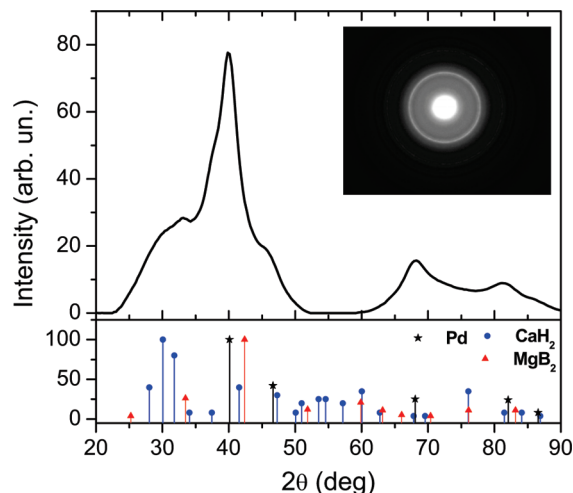

Figure 6. (top) SAED pattern for a 30 nm MgB_2 + CaH_2 codeposited film covered with 4 nm of Pd. (bottom) Process diffraction treatment of the SAED pattern with indications of the CaH_2, MgB_2, and Pd powder diffraction files from the JCPDS calculated using $\lambda = 1.54$ Å.

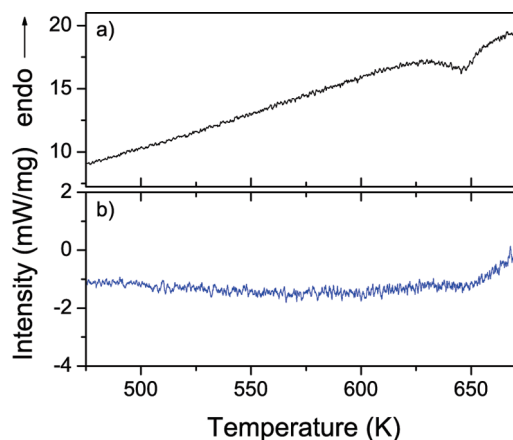**Figure 7.** Hydrogenation HP-DSC spectra of MgB_2 + CaH_2 + Ti (a) codeposited and (b) in a multilayer structure measured with a heating rate of 5 K/min during hydrogenation at 100 and 140 bar, respectively.

To quantify with more accuracy the amount of oxygen in the films as well as the presence of other impurities, MgB_2 films deposited using both pure Ar and a mixture of Ar/H_2 plasma have also been analyzed by means of RBS. To distinguish between the oxygen already present in the surface of the C substrates and the oxygen present in the MgB_2 films, we deposited a thick layer of yttrium or nickel as a buffer layer between the substrate and the film. Figure 5 shows the two oxygen peaks: one of them is labeled as O(C), which corresponds to oxygen on the surface of the C substrate, and the other peak is labeled as O(MgB_2), which corresponds to oxygen in the MgB_2 film. From the simulation of the experimental data, we find 6% of oxygen in the MgB_2 film independent of the composition of the plasma. Since the Pd top layer prevents quite efficiently the oxidation of the film, we have to assume that most of this oxygen comes from the MgB_2 target. For the composition, we obtain a ratio of 2:1.2 of B:Mg for films deposited in Ar plasma and 2:1 when using Ar/H_2. These values are consistent with the Mg in excess observed by means of XPS in the films deposited under Ar plasma. MgB_2 films were also analyzed by TEM. SAED patterns from a 30 nm film deposited using an Ar/H_2 plasma and covered with 4 nm of Pd do not show any crystalline phase apart from the Pd top layer (not shown). The presence of H_2 during the deposition probably prevents the growth of the crystal domains as was previously observed for in situ deposited MgH_2[17] and Mg_2NiH_4.[18] Although the stoichiometry is correct and previous studies showed that it is possible to synthesize MgB_2 under hydrogen pressure,[57] no confirmation for the formation of MgB_2 or other phases such as MgH_2 could be extracted from the TEM measurements. SAED patterns were also obtained from 30 nm thick MgB_2 + CaH_2 co-sputtered films (see Figure 6). In this case, as for the pure MgB_2 film, no signal was obtained from the MgB_2 phase and only the diffraction peaks from Pd and CaH_2 were identified. The formation of a $(Mg_xCa_{1-x})B_2$ phase, as some theoretical

studies predict,[58] cannot be totally discarded although part of the Ca was found in the hydride form.

Hydrogenation Treatment. To explore the formation of the $Ca(BH_4)_2$ compound during hydrogenation, we use two different configurations: a multilayer structure and co-sputtered films. The hydrogenation treatment of the co-sputtered films is performed in a HP-DSC with a constant hydrogen pressure of 100 bar and a heating rate of 5 K/min up to 773 K. The curve is shown in Figure 7a. We obtain a clear exothermic reaction with an onset temperature of 628 K. This temperature is close to the values obtained by Barkhordarian et al.[8] for the formation of $Ca(BH_4)_2$ + MgH_2 from CaH_2 and MgB_2 in bulk samples. This could be an indication for the formation of this phase in the cosputtered films, although a subsequent X-ray diffraction analysis of the samples shows no diffraction peaks from a newly formed phase. However, XRD measurements are not conclusive since the as-deposited films already present a fine microstructure not suitable to analyze by means of conventional X-ray diffraction. The samples are treated following the same hydrogenation treatment a second time and show no transformation. To discard reactions in the precursor films, the Cu substrate and pure MgB_2 and CaH_2 films are treated under the same conditions with no visible reaction. No significant structural change or signs of material

decomposition have been previously observed for MgB_2 after a hydrogenation treatment.[59] Assuming that the observed exothermic reaction corresponds to the formation of the Ca-$(BH_4)_2$ phase, then no significant improvement in the hydrogenation conditions has been obtained for the co-sputtered thin film structure.[8] We must consider then that the microstructure generated by co-sputtered thin films (optimal dispersion of material) is not advantageous for the formation of the calcium borohydride. This suggests that diffusion is not the limiting factor in this process. This is in agreement with recent findings by Bösenberg et al.[60] which point to the importance of the nucleation process of this class of materials.

The multilayer structure is submitted to an equivalent hydrogenation treatment with a temperature ramp of 5 K/min up to 673 K and 140 bar of hydrogen pressure. Figure 7b shows the curve obtained after the subtraction of a baseline corresponding to a repetition of the same hydrogenation treatment. In this case, the curve presents a small inflection around 643 K although it is almost indistinguishable from the noise. In the case of a multilayer structure, the reaction is expected to take place in the interfaces in contrast to the co-sputtered sample where the reaction can take place in the whole film at the same time. When a limitation in the diffusion of the species exists, as in this case, probably the new phase cannot grow farther than the interface where the reactant phases are in contact. This way, there is only a small amount of matter involved in the reaction, and no peak can be observed for these multilayers with the resolution of a conventional DSC.

Conclusions

Thin films of CaH_2 and NaH have been successfully deposited for the first time by means of reactive RF sputtering using a mixture of Ar/H_2 plasma. The optical response of the hydride films has been measured by optical spectrophotometry and has been simulated using the dielectric functions previously calculated using first principles at $GW_0 + BSE$ level with excitonic effects included. The agreement between the experimental and the simulated curves proves the effectiveness of the method for the analysis of hydride thin films and proves that the calculation of the dielectric functions reproduces with accuracy the optical band gap of the hydrides.

The formation of the $Ca(BH_4)_2$ phase has been investigated in two different configurations, co-sputtered films and multilayers, using high-pressure DSC. When a co-sputtered film is submitted to a high-pressure hydrogenation treatment, it presents an exothermic reaction at a temperature which is close to the one obtained for the formation of $Ca(BH_4)_2$ in bulk samples. This suggests that the reaction $CaH_2 + MgB_2 + 4H_2 \rightarrow Ca(BH_4)_2 + MgH_2$ takes place in the films although no further proof could be obtained since the new phase could not be observed by means of X-ray diffraction. When hydrogenating CaH_2-MgB_2 multilayers under similar conditions, the curve shows a small inflection around the same temperature, but the signal is too weak to confirm that the reaction is taking place. From the high temperature$-$pressure at which this transformation takes place in both co-sputtered and multilayered thin films, we can conclude that the microstructure generated by thin films does not represent a significant advantage. Diffusion, therefore, does not appear to be the main limiting factor in this process leaving the nucleation process as the main obstacle for the synthesis of calcium borohydride at low pressure and temperature.

Supporting Information Available: Dielectric functions of CaH_2, pure Ca, and $Ca(OH)_2$ calculated as described in the Computational Methods section. This material is available free of charge via the Internet at http://pubs.acs.org/.

References and Notes

(1) Vajo, J. J.; Olson, G. L. *Scr. Mater.* **2007**, *56*, 829–834.

(2) Dornheim, M.; Doppiu, S.; Barkhordarian, G.; Boesenberg, U.; Klassen, T.; Gutfleischa, O.; Bormann, R. *Scr. Mater.* **2007**, *56*, 841–846.

(3) Chen, P.; Zhu, M. *Mater. Today* **2008**, *11*, 36.

(4) Mao, J.; Yu, X.; Guo, Z.; Liu, H.; Wu, Z.; Ni, J. *J. Alloys Compd.* **2009**, *479*, 619–623.

(5) S.Walker, G.; Grant, D. M.; Price, T. C.; Yu, X.; Legrand, V. *J. Power Sources* **2009**, *194*, 1128–1134.

(6) Hu, J. Z.; Kwak, J. H.; Yang, Z.; Wan, X.; Shaw, L. L. *Appl. Phys. Lett.* **2009**, *94*, 141905.

(7) Bösenberg, U.; Doppiu, S.; Mosegaard, L.; Barkhordarian, G.; Eigen, N.; Borgschulte, A.; Jensen, T. R.; Cerenius, Y.; Gutfleisch, O.; Klassen, T.; Dornheim, M.; Bormann, R. *Acta Mater.* **2007**, *55*, 3951–3958.

(8) Barkhordarian, G.; Jensen, T. R.; Doppiu, S.; Bsenberg, U.; Borgschulte, A.; Gremaud, R.; Cerenius, Y.; Dornheim, M.; Klassen, T.; Bormann, R. *J. Phys. Chem. C* **2008**, *112*, 2743.

(9) Kim, Y.; Reed, D.; Lee, Y. S.; Lee, J. Y.; Shim, J. H.; Book, D.; Cho, Y. W. *J. Phys. Chem. C* **2009**, *113*, 5865.

(10) Lim, J.-H.; Shim, J.-H.; Lee, Y.-S.; Choa, Y. W.; Lee, J. *Scr. Mater.* **2008**, *59*, 1251–1254.

(11) Vajo, J. J.; Skeith, S. L.; Mertens, F. *J. Phys. Chem. B* **2005**, *109*, 3719–3722.

(12) Barkhordarian, G.; Klassen, T.; Dornheim, M.; Bormann, R. *J. Alloys Compd.* **2007**, *440*, L18–L21.

(13) Kim, Y.; Reed, D.; Lee, Y.-S.; Shim, J.-H.; Han, H. N.; Book, D.; Cho, Y. W. *J. Alloys Compd.* **2010**, *492*, 597.

(14) Rnnebro, E.; Majzoub, E. H. *J. Phys. Chem. B* **2007**, *111*, 12045.

(15) Niemann, M. U.; Srinivasan, S. S.; Kumar, A.; Stefanakos, E. K.; Goswami, D. Y.; McGrath, K. *Int. J. Hydrogen Energy* **2009**, *34*, 8086–8093.

(16) Lee, J. Y.; Ravnsbæk, D.; Lee, Y.-S.; Kim, Y.; Cerenius, Y.; Shim, J.-H.; Jensen, T. R.; Hur, N. H.; Cho, Y. W. *J. Phys. Chem. C* **2009**, *113*, 15080–15086.

(17) Westerwaal, R. J.; Broedersz, C. P.; Gremaud, R.; Slaman, M.; Borgschulte, A.; Lohstroh, W.; Tschersich, K.; Fleischhauer, H. P.; Dam, B.; Griessen, R. *Thin Solid Films* **2008**, *516*, 4351.

(18) Westerwaal, R. J.; Slaman, M.; Broedersz, C. P.; Borsa, D. M.; Dam, B.; Griessen, R.; Borgschulte, A.; Lohstroh, W.; Kooi, B.; ten Brink, G.; Tschersich, K. G.; Fleischhauer, H. P. *J. Appl. Phys.* **2006**, *100*, 063518.

(19) Engbaek, J.; Nielsen, G.; Nielsen, J. H.; Chorkendorff, I. *Surf. Sci.* **2006**, *600*, 1468.

(20) Filippi, M.; Rector, J. H.; Gremaud, R.; van Setten, M. J.; Dam, B. *Appl. Phys. Lett.* **2009**, *95*, 121904.

(21) Chatbi, H.; Vergnat, M.; Marchal, G. *Appl. Phys. Lett.* **1994**, *64*, 1210.

(22) Thompson, G. B.; Allred, D. D. *J. X-Ray Sci. Technol.* **1997**, *7*, 159–170.

(23) Ostenfeld, C. W.; Davies, J. C.; Vegge, T.; Chorkendorff, I. *Surf. Sci.* **2005**, *584*, 17–26.

(24) van Setten, M. J.; Popa, V. A.; de Wijs, G. A.; Brocks, G. *Phys. Rev. B* **2007**, *75*, 035204.

(25) van Setten, M. J.; Gremaud, R.; de Wijs, G. A.; Brocks, G.; Kresse, G.; Dam, B.; Griessen, R. Karlsruhe Institute of Technology, 2010, unpublished.

(26) Micunek, R.; Plecenik, A.; Kus, P.; Zahoran, M.; Tomasek, M.; Plecenik, T.; Gregor, M.; Stefecka, M.; Jacko, V.; Gregus, J.; Grancic, B.; Kubinec, M.; Mahel, M. *Physica C* **2006**, *435*, 78–81.

(27) Santoni, A.; Vetrella, U. B.; Celentano, G.; Gambardella, U.; Mancini, A. *Appl. Phys. A: Mater. Sci. Process.* **2007**, *86*, 485–490.

Formation of Reactive Hydride Composites

J. Phys. Chem. C, Vol. 114, No. 32, 2010 **13901**

(28) Akinaga, M.; Umeda, S.; Hasegawa, H.; Shirasawa, T. *Physica C* **2003**, *388−389*, 119–120.

(29) Giunchi, G. *Int. J. Mod. Phys. B* **2003**, *17*, 453.

(30) Labar, J. L. *Ultramicroscopy* **2005**, *103*, 237.

(31) Doolittle, L. R. *Nucl. Instrum. Methods Phys. Res. B* **1985**, *15*, 227.

(32) Bogdanovi, B.; Schwickardi, M. *J. Alloys Compd.* **1997**, *253−254*, 1–9.

(33) Kresse, G.; Furthmüller, J. *Phys. Rev. B* **1996**, *54*, 11169.

(34) Kresse, G.; Furthmüller, J. *Comput. Mater. Sci.* **1996**, *6*, 15.

(35) Kresse, G.; Hafner, J. *Phys. Rev. B* **1993**, *47*, 558.

(36) Kresse, G.; Joubert, D. *Phys. Rev. B* **1999**, *59*, 1758.

(37) Blöchl, P. E. *Phys. Rev. B* **1994**, *50*, 17953.

(38) Bergsma, J.; Loopstra, B. O. *Acta Crystallogr.* **1962**, *15*, 92.

(39) Perdew, J. P.; Chevary, J. A.; Vosko, S. H.; Jackson, K. A.; Pederson, M. R.; Singh, D. J.; Fiolhais, C. *Phys. Rev. B* **1992**, *46*, 6671.

(40) Hedin, L. *Phys. Rev.* **1965**, *139*, A796.

(41) Hedin, L.; Lundqvist, B. I. *J. Phys. C* **1971**, *4*, 2064.

(42) Hedin, L. *J. Phys.: Condens. Matter* **1999**, *11*, R489.

(43) Shishkin, M.; Kresse, G. *Phys. Rev. B* **2006**, *74*, 035101.

(44) Shishkin, M.; Kresse, G. *Phys. Rev. B* **2007**, *75*, 235102.

(45) Fuchs, F.; Furthmüller, J.; Bechstedt, F.; Shishkin, M.; Kresse, G. *Phys. Rev. B* **2007**, *76*, 115109.

(46) Shishkin, M.; Marsman, M.; Kresse, G. *Phys. Rev. Lett.* **2007**, *99*, 246403.

(47) van Setten, M. J.; Er, S.; Brocks, G.; de Groot, R.; de Wijs, G. A. *Phys. Rev. B* **2009**, *79*, 12117.

(48) Harl, J.; Kresse, G.; Sun, L. D.; Hohage, M.; Zeppenfeld, P. *Phys. Rev. B* **2007**, *76*, 035436.

(49) Weaver, J. H.; Gupta, M.; Paterson, D. T. *Solid State Commun.* **1984**, *51*, 805–808.

(50) Theiss, W. *SCOUT Thin Film Analysis Software Handbook, Hard and Software, Aachen*; 2000; www.mtheiss.com.

(51) Bruggeman, D. A. G. *Annu. Phys.* **1935**, *24*, 636–664.

(52) Whited, R.; Walker, W. *Phys. Rev. Lett.* **1969**, *22*, 1428.

(53) Talapatra, A.; Bandyopadhyay, S. K.; Sen, P.; Barat, P.; Mukherjee, S.; Mukherjee, M. *Physica C* **2005**, *419*, 141–147.

(54) Garg, K. B.; Chatterji, T.; Dalela, S.; Heinonnen, M.; Leiro, J.; Dalela, B.; Singhal, R. K. *Solid State Commun.* **2004**, *131*, 343–347.

(55) Aswal, D. K.; Muthe, K. P.; Singh, A.; Sen, S.; Shah, K.; Gupta, L. C.; Gupta, S. K.; Sahni, V. C. *Physica C* **2001**, *363*, 208–214.

(56) Serquis, A.; Zhu, Y. T.; Peterson, D. E.; Mueller, F. M.; Schulze, R. K.; Nesterenko, V. F.; Indrakanti, S. S. *Appl. Phys. Lett.* **2002**, *80*, 4401.

(57) Nakamori, Y.; Orimo, S.; Ekino, T.; Fujii, H. *J. Alloys Compd.* **2002**, *335*, L21–L24.

(58) Wu, X. S.; Gao, J. *Physica C* **2005**, *418*, 151–159.

(59) Flambaum, V. V.; Stewart, G. A.; Russell, G. J.; Horvat, J.; Dou, S. X. *Physica C* **2002**, *382*, 213–216.

(60) Bosenberg, U.; Vainio, U.; Pranzas, P. K.; von Colbe, J. M. B.; Goerigk, G.; Welter, E.; Dornheim, M.; Schreyer, A.; Bormann, R. *Nanotechnology* **2009**, *20*, 204003.